Available online at www.sciencedirect.com
ScienceDirect
Nuclear Instruments and Methods in Physics Research A 566 (2006) 746–756
NUCLEAR INSTRUMENTS & METHODS IN PHYSICS RESEARCH Section A
www.elsevier.com/locate/nima

A magnetic trap for antihydrogen confinement

W. Bertsche[a], A. Boston[b], P.D. Bowe[c], C.L. Cesar[d], S. Chapman[a], M. Charlton[e], M. Chartier[b], A. Deutsch[a,f], J. Fajans[a,f], M.C. Fujiwara[g], R. Funakoshi[h], K. Gomberoff[a,f], J.S. Hangst[c], R.S. Hayano[h], M.J. Jenkins[e], L.V. Jørgensen[e], P. Ko[a], N. Madsen[e], P. Nolan[b], R.D. Page[b], L.G.C. Posada[h], A. Povilus[a], E. Sarid[i], D.M. Silveira[d], D.P. van der Werf[e,*], Y. Yamazaki[j] (ALPHA Collaboration) , B.Parker[k], J.Escallier[k], A.Ghosh[k]

[a]*Department of Physics, University of California at Berkeley, Berkeley, CA 94720-7300, USA*
[b]*Department of Physics, University of Liverpool, Liverpool L69 7ZE, UK*
[c]*Department of Physics and Astronomy, University of Aarhus, DK-8000 Aarhus C, Denmark*
[d]*Instituto de Física, Universidade Federal do Rio de Janeiro, Rio de Janeiro 21945-970, Brazil*
[e]*Department of Physics, University of Wales Swansea, Swansea SA2 8PP, UK*
[f]*Lawrence Berkeley National Laboratory, Berkeley, CA 94720, USA*
[g]*TRIUMF, 4004 Wesbrook Mall Vancouver, BC Canada V6T 2A3*
[h]*Department of Physics, University of Tokyo, Tokyo 113-0033, Japan*
[i]*Department of Physics, NRCN-Nuclear Research Center Negev, Beer Sheva IL-84190, Israel*
[j]*Atomic Physics Laboratory, RIKEN, Saitama 351-0198, Japan*
[k]*Brookhaven National Laboratory, Upton, NY 11973, USA*

Received 7 July 2006; accepted 8 July 2006
Available online 2 August 2006

Abstract

The goal of the ALPHA collaboration at CERN is to test CPT conservation by comparing the 1S–2S transitions of hydrogen and antihydrogen. To reach the ultimate accuracy of 1 part in 10^{18}, the (anti)atoms must be trapped. Using current technology, only magnetic minimum traps can confine (anti)hydrogen. In this paper, the design of the ALPHA antihydrogen trap and the results of measurements on a prototype system will be presented. The trap depth of the final system will be 1.16 T, corresponding to a temperature of 0.78 K for ground state antihydrogen.

PACS: 36.10.−k; 34.8DLx; 52.20Hv

Keywords: Antihydrogen; Antiprotons; Positrons; Penning trap; Neutral trap

1. Introduction

Based on locality, Lorentz invariance and unitarity, the CPT theorem is one of the cornerstones of Quantum Field Theory and the Standard Model [1]. The theorem states that the laws of physics should be invariant when the spatial coordinates, charge, and time change sign simultaneously. As a consequence of CPT conservation, particles and antiparticles should have identical masses and lifetimes and identical but opposite charges and magnetic moments. Moreover, there should be no difference between the energy levels (for example the gross, fine and hyperfine structures and the Lamb shifts) of atoms made from matter and antimatter.

A direct test of the CPT theorem can be made by comparing the 1S–2S electronic transitions of hydrogen and antihydrogen in a magnetic field [2]. The long lifetime of the metastable 2S level means that a measurement limit of 10^{-18} [3] between the relative differences of the 1S and 2S intervals may ultimately be feasible. Other schemes

*Corresponding author. Tel.: +44 1792 513053; fax: +44 1792 295324.
E-mail address: D.P.van.der.Werf@Swansea.ac.uk (D.P. van der Werf).

0168-9002/$ - see front matter © 2006 Elsevier B.V. All rights reserved.
doi:10.1016/j.nima.2006.07.012

have been proposed for initial spectroscopy using the 2S–nD ($n \approx 10$) transitions [4].

Recently two collaborations (ATHENA and ATRAP) working at CERN's Antiproton Decelerator (AD) facility have efficiently created low energy but untrapped antihydrogen atoms in a nested Penning trap environment [5–7]. Although these results are important milestones towards testing CPT conservation, high precision CPT tests can only be performed with trapped antihydrogen atoms.

In the schemes for antihydrogen production used to date by ATHENA, in which antiprotons are injected epithermally into a positron plasma, the typical measured formation temperature is at least 15 K in the radial direction and 150 K axially [8]. From measurements of weakly bound antihydrogen ATRAP derived axial velocities corresponding to a temperature of about 2000 K [9]. Theoretical simulations of antiproton–positron mixing under similar conditions to those encountered in ATHENA and ATRAP also point to antihydrogen formation on timescales resulting in epithermal kinetic energies [10]. Another formation method has been demonstrated using Rydberg positronium atoms [11], which may in principle yield colder antihydrogen.

A number of variants on the nested trap scheme have recently been proposed by the new ALPHA antihydrogen collaboration (Antihydrogen Laser PHysics Apparatus) [12], aimed at producing antihydrogen with lower kinetic energies, though these methods have not yet been realized. It was also shown in Ref. [12] that assuming a positron plasma at a temperature of 4 K and a density of $5 \times 10^6\,\mathrm{cm}^{-3}$, and using a mixing scheme similar to that developed by ATHENA, around 5% of the antihydrogen atoms emerge with kinetic energy equivalent temperatures below 0.5 K.

Lasers which can cool and trap antihydrogen have not yet been developed. Consequently, following the very earliest suggestions in this field [13,14], most of the proposed antiatom trapping schemes have relied on magnetic confinement (see Refs. [15–17]). Some fraction [18] of the antiatoms will be in diamagnetic, low-field seeking spin states, and these antiatoms can be trapped in a three-dimensional magnetic minimum. The well depth for antiatoms in a magnetic trap is proportional to the difference between the minimum magnetic field magnitude, B_0, at the center of the well, and the magnetic field magnitude, B, at the lowest saddle point surrounding the minimum. The well depth can be expressed as a potential energy, $kT = \mu(B - B_0)$, where, for ground-state (anti)hydrogen, μ is the Bohr magneton. Thus, only atoms with kinetic energies corresponding to temperatures of $0.67\,\mathrm{K\,T}^{-1}$ and lower will be trapped.

To enhance the trapped fraction of antiatoms, the well depth should be as deep as is technically feasible. The design proposed here has a well depth of approximately 0.78 K for ground-state antihydrogen. The well depth for trappable excited antihydrogen, like that formed by both ATHENA [19] and ATRAP [7], is significantly deeper. Since some center-of-mass cooling occurs as the antihydrogen decays to its ground state, this may increase the trapping fraction [20]. However, only trapped, ground-state antihydrogen can be easily used for precision spectroscopy.

In this paper, we present the design of the magnet system to be used by the ALPHA collaboration [12]. We begin with the magnet design, wire choice, and construction method in Section 2. The calculation methods are explained in Section 3, whereafter we describe the design of a prototype system, and present the results from tests performed on it in Section 4. Quench protection will be briefly discussed in Section 5 and the main conclusions will be presented in Section 6.

2. Magnet design

We form our magnetic well with two mirror coils and a multipole coil. The mirror coils, which must be spaced at distances substantially greater than in a Helmholtz configuration, make the axial well, while the multipole coil provides the radial well. The fields from these coils are superimposed on a uniform solenoidal field, which is required to confine the charged positron and antiproton plasmas from which the antihydrogen is synthesized.

2.1. Design criteria

The magnet system must satisfy the following three major and one minor design criteria.

2.1.1. Major criterion: well depth

As discussed in Section 1, we need to maximize the magnetic well depth if we are to trap an appreciable number of antihydrogen atoms. It is relatively easy to make large mirror fields to plug the trap axially. Consequently, the limiting trap depth comes from the difference between the total field at the Penning trap electrode inner wall, and the trap axis. At the electrode wall, the multipole field B_w and the axial solenoidal field, B_z are orthogonal. Thus, we need to maximize

$$\Delta B = \sqrt{B_z^2 + B_w^2} - B_z. \tag{1}$$

The mirror field strength does not affect Eq. (1) directly, but the mirror coils also produce radial fields. Near the mirror coils, these radial fields will interact with the multipole radial fields, adding constructively at some azimuthal angles and destructively at others. Where the two add destructively there may be "holes" in the magnetic well, and the antihydrogen may be able to leak out [17]. The depth of the holes depends on the lengths and positions of the mirror coils and on the lengths of the end sections of the multipole. The end geometry must be carefully engineered to minimize the holes. (See Section 2.3.2 for more details.)

2.1.2. Major criterion: multipole order

The antiproton and positron plasmas must remain confined [17] if we are to synthesize antihydrogen. This requirement dictates the choice of multipole order. Neutral magnetic traps [21] typically use the so-called Ioffe–Pritchard configuration [22], which employs a quadrupole coil for the multipole. Such a quadrupole, with two mirror coils and a solenoid, is the simplest configuration that could possibly be used in an antihydrogen trap. However, it is not obvious that the positron and antiproton plasmas from which the antihydrogen is synthesized can be confined in this configuration. Common Penning traps rely on cylindrical symmetry to guarantee confinement [23], and this symmetry is broken by the multipolar field.

Whether or not the constituent plasmas will stay confined in the presence of a quadrupole has been much disputed. A number of experiments have addressed this issue and shown that, for relatively weak solenoidal fields and/or with small quadrupole to solenoidal field ratios, plasmas are not suitably confined [17,24–26]. Other work has suggested otherwise [27,28]. Recently, however, confinement measurements with field strengths approaching the magnitudes necessary for antihydrogen trapping have been performed [29]. These experiments have conclusively shown that quadrupoles sharply degrade the constituent confinement, and that quadrupolar fields cannot be used, particularly when the ratio of the quadrupole field $B_2(r_0)$ to solenoidal field at the plasma radius, r_0, exceeded about $B_2(r_0)/B_z \geqslant 0.05$ [12,29] for appropriate length plasmas. Aspects of these experiments have been confirmed by particle-in-cell (PIC) simulations [32].

The magnitude of the field of an infinitely long multipole of order s scales with radius r as

$$|B_s(r)| = K_s r^{s-1}, \tag{2}$$

where the K_s are constants and s defines the order of the multipole (e.g. a quadrupole for $s = 2$, a sextupole for $s = 3$, an octupole for $s = 4$, etc). In Fig. 1 we have plotted the field dependence for $s = 2$–5 where the field strength is normalized to unity at the electrode inner wall radius, r_w. The maximum field magnitude in a multipole occurs at the coil inner radius, and is proportional to the current density in the conductors there. With superconducting wires, the current density is, to first order, only dependent on the type of conductor and on the local magnetic field magnitude. Thus, to first order, the field at the wall of a multipole is independent of the multipole order [17]. This gives us considerable freedom to optimize the order.

While the maximum field, and hence the trapping depth, is roughly independent of the multipole order, the interior field is not. The higher the order of the multipole, the lower the interior field. The positron and antiproton plasmas extend only a small way to the trap wall. Consequently, for a given trap depth, they will be subject to smaller multipole fields as the multipole order is increased. The plasmas in ALPHA are envisaged to have radii of about $r_0 \leqslant 0.2 r_w$. If we assume that the maximum azimuthally asymmetric field

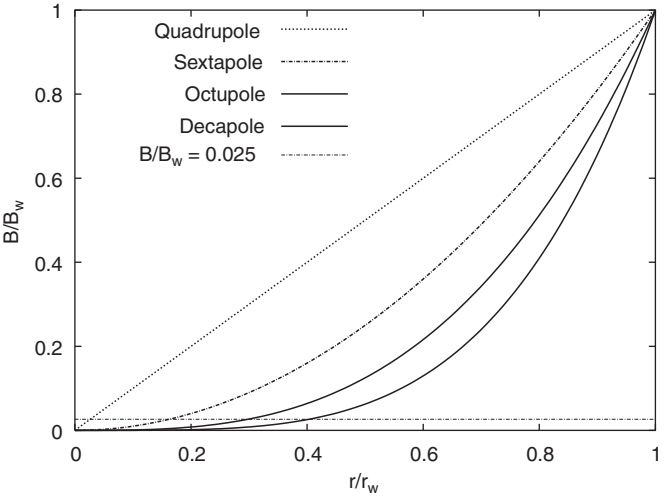

Fig. 1. Radial field dependence for $s = 2$–5 (quadrupole through decapole) normalized to unity at the electrode wall radius. The significance of the horizontal line is explained in the text.

that the plasmas can tolerate for higher order multipoles is similar to the maximum tolerable field for a quadrupole, we can extend our quadrupole tolerance limit to the more general limit $B_s(r_0)/B_z \geqslant 0.05$. This limit corresponds to the horizontal line in Fig. 1 (the multipole field at the wall is about twice the solenoidal field), and is satisfied by octupoles and higher multipoles for all radii less then $0.2 r_w$. It might, at first, seem preferable to use an order higher than an octupole. However, because the multipole support form, the vacuum wall, and the interior electrodes all have finite thickness, the trap wall radius will be significantly less than the coil inner radius. This causes the effective maximum field at the trap wall radius to be significantly reduced from the field at the coil radius, a reduction that increases sharply with the multipole order. We believe that an octupole is the best compromise between minimizing the field felt by the plasmas while still maintaining the neutral trap depth. Furthermore, limits on the bending radius of the superconducting wire also favor an octupole with our particular geometry.

2.1.3. Major criterion: material minimization

ALPHA will use a position sensitive particle detector to record the antiproton annihilation vertices. The detector will be placed just outside the magnet coils. The coils will scatter the charged pions which are emitted upon antihydrogen annihilation, thereby degrading the resolution of the detector. Thus, another design criterion is to minimize the material between the vacuum in the trap and the detector in order to minimize the scattering [30].

2.1.4. Minor criterion: magnet ramping

The presence of trapped antihydrogen can be inferred from its annihilation following release from the trap by quickly ramping down one of the magnets. The faster the magnet can be ramped, the higher the signal to noise ratio

against background events such as cosmic rays. Moreover, it is not yet known if plasmas can be injected while the multipole is energized, so ramping of the multipole after injecting could be necessary. The ramping speed will depend on the inductance of the magnets. Therefore, magnets wound with fewer turns of higher current cable are preferable.

2.2. Wire

We want our trap to be as deep as possible. Only superconducting magnets are sufficiently strong; neither copper nor permanent magnets are anywhere near strong enough. Niobium–Tin (NbSn) technology is too expensive and too difficult to form into an octupole, so our magnets are wound from Niobium–Titanium (NbTi). As with any superconducting technology, NbTi wires can only support a limited current before they become normal (see Fig. 2). This critical current density depends on the local transverse magnetic field at the wire. As discussed in Section 2.1.2, the multipole strength depends on the current density in the wires, so we need to maximize this.

Practical superconducting wires cannot be made from pure superconducting material; instead, they consist of superconducting filaments embedded in a copper matrix (see Fig. 3). In normal operation no current flows through the copper, but in the event of a quench (a superconducting to normal transition in some part of the coil), the copper carries the current around the region of superconducting material that turned normal. If the current were forced to flow through the normal superconductor, Joule heating could heat the superconductor up to temperatures where it would burn out, destroying the coil. The copper also makes the wire more stable; in the event of a very small, localized quench, the copper can carry the current around the quench and allow the superconductor to cool down and return to the superconducting state.

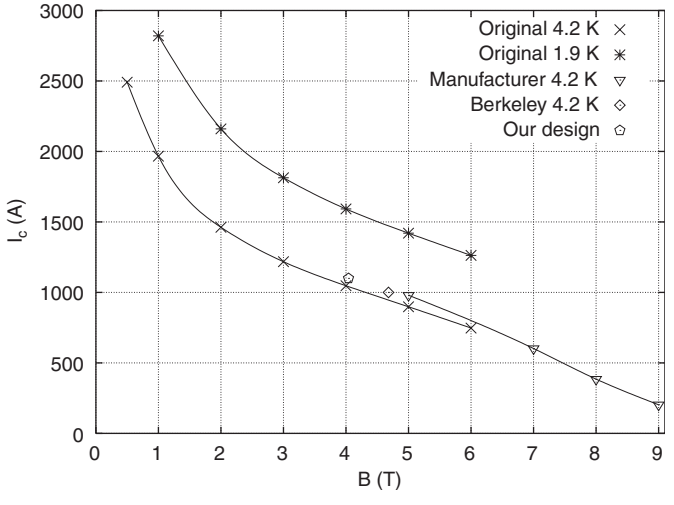

Fig. 2. Critical current at various magnetic fields for the 0.9:1 seven stranded Supercon wire cable bundle. The points marked "Berkeley" and "Our design" were taken with 0.33 mm wire; the remaining points were taken with very similar 0.303 mm wire. The two "Original" data sets were taken at the Brookhaven National Laboratory, while the "Manufacturer" data set was taken by Supercon. These three sets were taken with short wire samples, and set likely upper bounds on the performance of the wire when incorporated into a magnet. The "Berkeley" point comes from measurements of the prototype magnet at U.C. Berkeley, and is very close to the short sample performance when adjusted for the increased radius. The "Our design" point is located at ALPHA's intended operation point.

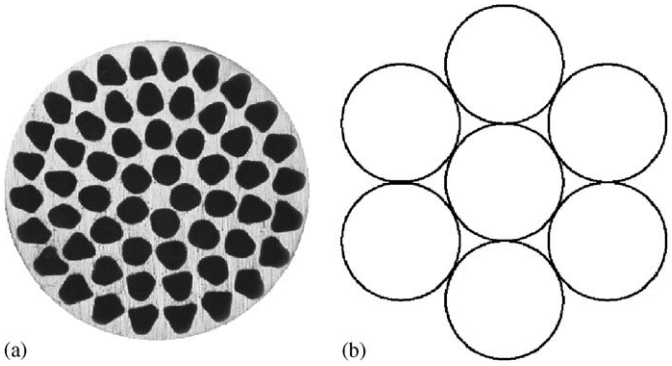

Fig. 3. Wire and cable configuration used in our magnets: (a) the superconducting wire showing the NbTi embedded in the copper matrix (photograph strand 56S53, courtesy of Supercon) [31] and (b) seven stranded cable configuration. The overall diameter of the cable, including insulation and *B*-stage epoxy, is 1.156 mm.

Typically, superconducting magnets are wound with wires with copper/superconductor (Cu/Sup) ratios of at least 1.6:1. However, the achievable current density is inversely proportional to the Cu/Sup ratio, because no current flows in the copper. This limits the field we can attain in our octupole. We can tolerate an occasional quench, and, as described later, we can prevent the octupole from burning out. Consequently, we have chosen a wire with the unusually low Cu/Sup ratio of 0.9:1 (Fig. 3a) manufactured by Supercon [31]. Rather than using this wire directly, we had it woven into a seven stranded cable, as shown in Fig. 3b. This reduces the manufacturing complexity of the magnet (fewer layers) and its inductance, at the expense of increasing the magnet current. Fig. 2 shows the short sample currents for this cable.

2.3. Octupole winding pattern

We project that the critical current in our octupole will be about 1100 A (see Fig. 2). This implies a surface current density of about 8800 A mm^{-1} for a one layer octupole. To generate fields of several Tesla, the surface current density must be several times greater. Thus, our octupole must have multiple layers. However, the contributions from the outer layers fall off quickly because the field falls off as r^3. To balance our need for a large field with our need to minimize the material in the magnet, we chose eight layers.

Our octupole is wound following a serpentine pattern (see Fig. 4), rather than the more common racetrack pattern. By reversing the winding direction and azimuthally

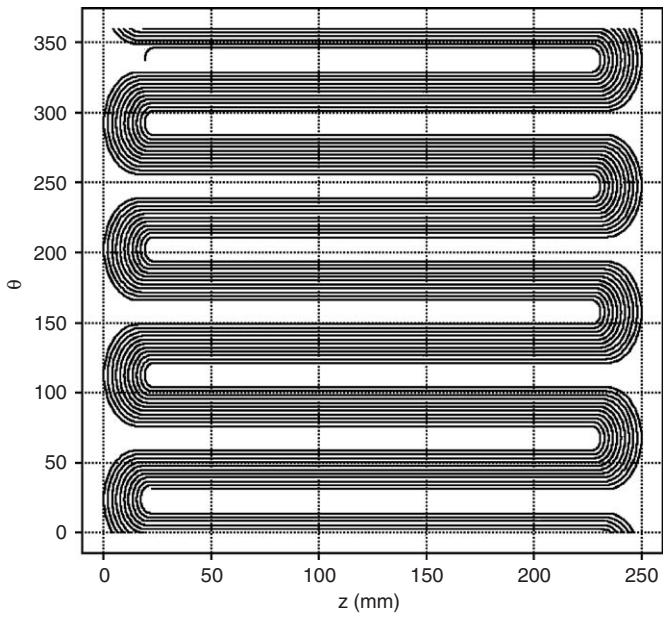

Fig. 4. Serpentine pattern used to wind multipoles. Conventional cylindrical coordinates are used.

staggering adjacent layers by 45°, we direct the azimuthal current at the octupole ends in alternate directions. This cancels almost all the axial field that would occur if we did not stagger the ends. So the axial well is formed by the mirror coils alone, and the well is much easier to manipulate. Without staggered ends, we would have to add a bucking coil, or carefully adjust and possibly reverse drive the mirror coil currents to null the axial well. This would increase the complexity of our system and possibly dangerously increase the forces on our coil form. As an added benefit, staggering reduces the mutual inductances between the mirror coil and the octupole.

In addition to staggering the coils on successive layers, we adjust the number of turns and turn spacing in each winding layer to get as perfect a $\cos 4\theta$ distribution as possible by minimizing the next allowed $\cos 12\theta$ field harmonic term. Since higher than octupole order field harmonics only increase the peak field at the conductor without adding as much field inside the trap we are able to operate a stronger trap at higher operating current by minimizing such higher-order terms. We used 11 (innermost), 11, 13, 13, 15, 15, 15, and 15 (outermost) wires in each leg on successive layers. The calculated maximum B_{norm} (see Section 3) for the octupole running at its maximum current of 1100 A, when all the other elements in the systems are energized, is 4.04 T. This is plotted in Fig. 2 and is within the critical current for the octupole.

2.3.1. Mechanical forces

The mirror and octupole coils press outward with substantial force when energized. Calculations show that the resultant pressures may exceed 40 bar. To contain these pressures, the coil is wrapped with pre-tensioned fiberglass *s*-glass roving. To provide a safety margin, the tension in these tapes exceeds the calculated maximum pressure by 25%. When the coils are de-energized, there is no counterbalance for the pressure from the tapes, and the pressure must be supported by the coil form. The conversion of liquid helium to gaseous helium in a quench can further increase the inward pressure. Obviously, the collapse of the magnet form would be catastrophic. However, we cannot make the form arbitrarily thick because doing so reduces the effective octupole field at the trap wall. For instance, for a coil inner radius of 25 mm, and a net form, wall, and electrode thickness of 2.5 mm, the useful field is reduced by 27%. After carefully considering all the forces, we have set the form thickness to 1.25 mm of 316 LN stainless steel. To further minimize the thickness penalty, we have wound the octupole directly on the vacuum wall. This has the additional advantage of ensuring that the vacuum wall will be at 4.2 K, and consequently, will be an excellent cryopump.

2.3.2. Trap holes

Placing the mirror coils over the straight wire region of the octupole would be desirable as it would keep the transition region short. Unfortunately, it would also increase the outward pressure when the coils are energized, and would require us to thicken the coil form to compensate for the correspondingly higher tension *s*-glass wrap. Consequently, we placed the mirror coils outward so they overlap only the end turns of the octupole. Still, we need to strengthen the coil form by thickening it to 2.5 mm just beyond the octupole.

Placing the mirror coils outwards opens up holes in the magnetic well. We choose the optimal position by trading off the well depth loss from the holes with the well depth loss that results from thickening the form. Fig. 5 shows $|B|$ (all magnets are energized) as a function of the axial coordinate, z, for a number of radii spaced 1 mm apart. Each figure shows the field at a different azimuthal angle, θ. As can be seen in Fig. 5a ($-22.5°$) and 5c (22.5°), the smallest field along the well boundary is at the saddles near the mirror coils; it is through these holes that antihydrogen may escape. The lowest saddle has a value of 2.25 T. The lowest field within the magnet system has a value of 1.09 T giving the trap a well depth of 1.16 T, corresponding to a temperature of 0.78 K for ground state antihydrogen.

2.4. Mirror coils

The two mirror coils have four layers of 30 turns each. The average radius of the coils is about 43.5 mm, and the coil center to coil center separation is 274 mm. The coils will be driven by a current of 750 A. The mirror coils are wound from the same wire as the octupoles. Since the maximum field transverse to the mirror coil wires is about 3.7 T, this current is well below the critical current in the wire. The extra material thickness in the mirror region will degrade the imaging of the particles that emerge

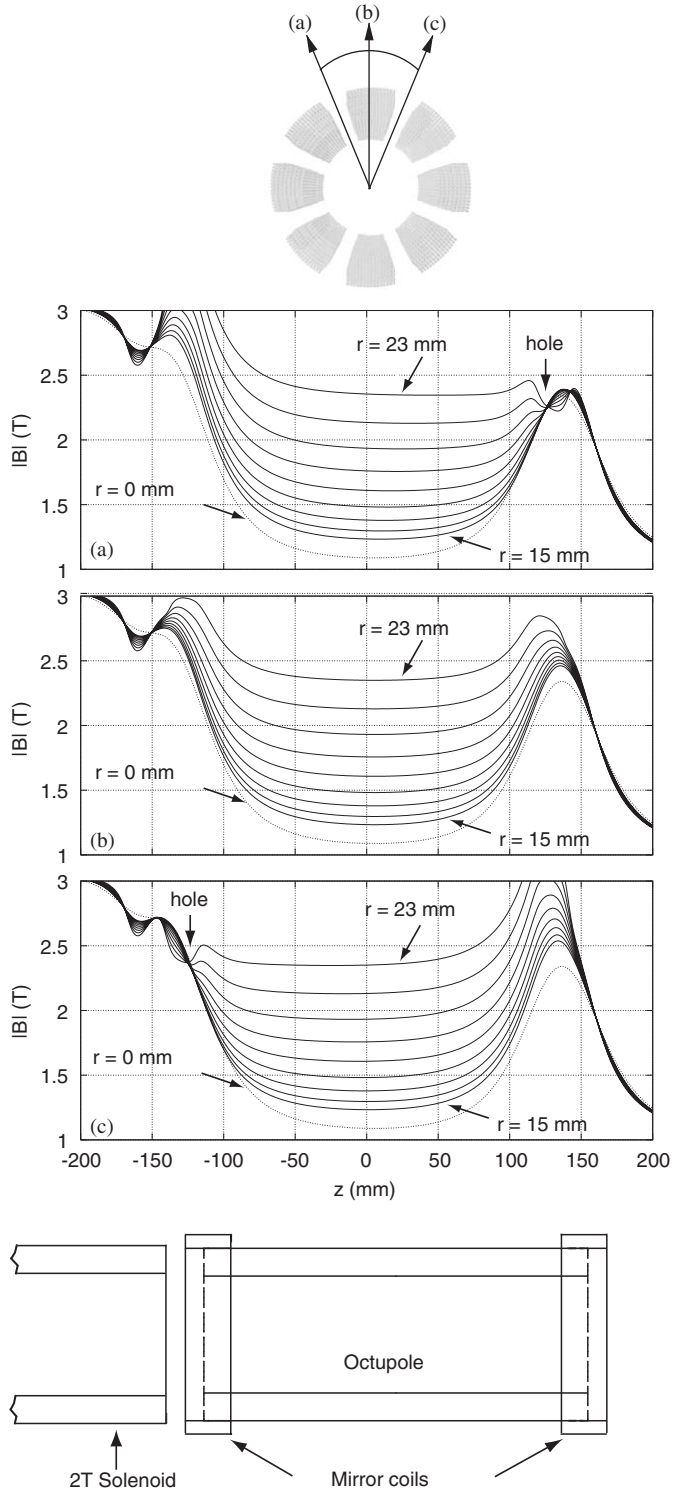

Fig. 5. The top picture is an axial view of a cross section in the middle of the magnet system indicating the azimuthal angles for the planes for (a), (b) and (c).These three plots show the total field for a number of different radii as function of z. The radius for subsequent solid lines differs by 1 mm: (a) $-22.5°$; (b) $0°$; and (c) $22.5°$ (see text). The bottom picture shows the schematic magnetic assembly.

from nearby annihilation events, but, as the mirrors are outside of the antihydrogen synthesis region, the degradation is less critical.

2.5. Antiproton capture solenoid

In ATHENA the antiprotons, coming from the CERN AD ring, were captured in a 3 T solenoidal field [19]. On the other hand, a low solenoidal field is preferred in order to maximize the well depth (see Eq. (1)). Therefore, a compromise has been made by surrounding the mirror and octupole by a large-diameter, external solenoid [33] that generates the 1 T field used to confine the positron and antiproton plasmas and adding an extra 2 T small-diameter internal solenoid adjacent to one of the mirrors (see Fig. 6). This provides a $\sim$300 mm long, 3 T region to catch the antiprotons. After capture and cooling, the antiprotons will be transferred to the 1 T region under the octupole. The eight layer internal solenoid will be made from the same cable as the octupole. The antiproton capture region extends beyond the flat field region of the large-diameter solenoid; the internal solenoid compensates for this fall-off by adding several extra turns and two layers at its far end. The 230 A current needed to drive the internal solenoid is well below the wire's critical current in the 3 T maximum transverse field to which it is exposed.

2.6. Winding method

Because we use a serpentine pattern, stagger the ends, and increase the number of turns per layer, our octupole could not be wound using conventional techniques on a machined form. Instead, it was built using a unique technique developed at the Brookhaven National Laboratory, wherein the wire is initially ultrasonically glued into place, and then permanently secured with G-10 spacers (in winding gaps), *B*-stage epoxy, and fiber overwraps [34]. This technique allows the wires to be placed in almost any pattern, with complete freedom to change the pattern between layers. The first layer of the octupole is shown in Fig. 7. The BNL technique eliminates the need for steel collars to contain the magnetic forces as is commonly done in high field accelerator magnets. Such collars would preclude the detection of the annihilation products of the antiparticles.

The mirror coils and solenoid are wound using more conventional techniques.

2.7. Field errors

Normally Penning traps intended to confine high-density plasmas are meticulously designed to minimize field errors [35]. However, the octupole is such a gross deviation from the ideal, azimuthally symmetric fields that minor field errors are of relatively little importance. As described in Section 2.3, field errors that come from design deviations from the ideal $\cos 4\theta$ current distribution are unimportant. However, deviations that come from inaccurate wire placement could result in dangerous lower order multipole fields. We have adopted the criterion that the field that results from these errors should be less than 10% of the

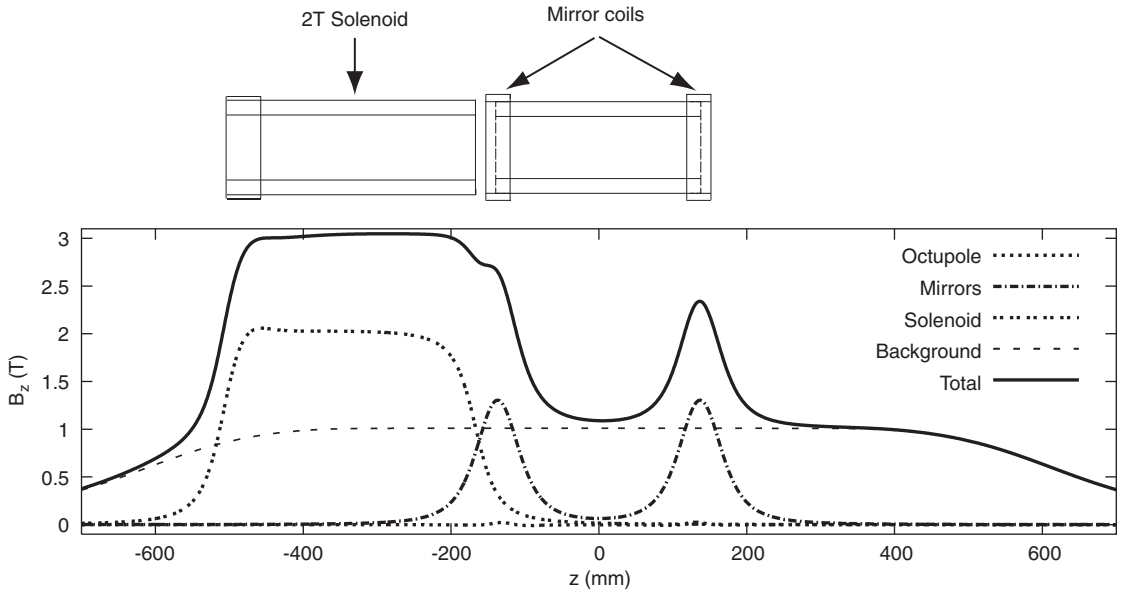

Fig. 6. Magnetic field on axis for the magnet assembly including the 1 T background field from the large-diameter external solenoid (see Section 2.5).

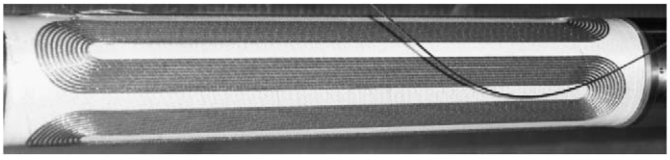

Fig. 7. First layer of the octupole. The wires are held in place by ultrasonic bonding; the spacers, *B*-stage epoxy, and fiber overwraps have not yet been applied.

octupole field at the putative plasma radius of 10 mm. This is a relatively easy manufacturing criterion to meet.

The current leads for one of the mirror coils and for the solenoid must pass over the octupole. These leads will produce a dipole error field. We have studied the effect of these leads by modeling them as two long filaments, separated by the wire diameter, at a radius of 44 mm, carrying 750 A in opposite directions. We calculated the total field from the octupole and these filaments at a radius of 10 mm at $z = 0$ over 360°. The effect from the leads is within the 10% criterion mentioned above.

3. Calculations

To optimize the design of our octupole we needed to calculate the critical fields and currents, and the magnetic forces for each candidate design. We used the TOSCA/OPERA3D package [36], together with purpose-written programs to find these quantities. As all the materials in the magnet system have relative magnetic permeabilities of one, the fields can be calculated from the Biot–Savart law. The multipole is implemented into TOSCA/OPERA3D, using their BR20 conductor model, by dividing the multipole into long straight sections and a number of small sections for each turn. The mirror coils are modeled as one conductor or, when calculating critical currents and forces inside the coil, as a number of current loops equal to the number of turns. In the latter case the current loops are divided into a number of segments, again modeled using the BR20 conductor. Convergence checks as a function of the number of sections have been performed. In a number of cases the calculated multipole fields have been compared with models in OPERA2D. The mirror coil calculations have been checked using analytic models. Moreover, the calculated inductance of the prototype (see Section 4) agrees to within 1% with the measured value.

The multipole will quench if any wire segment exceeds its critical current. Since the critical current depends on the local magnetic field magnitude, we need an accurate field map. We find that the highest fields are in the vicinity of the mirror coils. Small changes in the mirror design, and in the shape of the ends of the multipole, can significantly affect the critical current. Note that fields parallel to the current in a wire do not influence the value of the critical current. Therefore, we use the normal field magnitude, B_{norm}, to determine the critical current. Further, the field used in the short sample measurements is defined to include only the external field, not the field from the current in the wire itself.

4. Prototype system

As discussed in Section 2.2, our wire has an unusually low Cu/Sup ratio. Consequently, we built a prototype magnet to validate the short sample critical current measurements (see Fig. 2), and to test the wire's stability in a real system. We also used the prototype to measure hot spot temperatures and velocities during induced quenches, and to see if the wire was damaged by repeated quenching.

4.1. Design

The two layer octupole prototype magnet has an inner radius of 25 mm and a length of about 350 mm. The octupole incorporates spot heaters, used to induce quenches, on the leads and on the outermost turn of the second layer. It also incorporates voltage taps for measuring the voltage drop across layers to detect quenches, as well as taps for measuring quench velocities. Wound on top of the octupole is a two layer, 120 turn, mirror coil of length 135 mm. The mirror coil is made from a seven stranded (1.78:1) Cu/Sup cable, with the core wire made of copper, to study its ramping behavior. The length of the mirror coil was chosen such that its inductance is similar to that of the ALPHA mirror coils.

4.2. Results

The prototype octupole does not self-quench when driven by the maximum current, 1000 A, that its supply can produce. Nor does it quench when immersed in the field from a 4.2 T external solenoid. However, it does quench in the field of the external solenoid and the prototype mirror. Consequently we measured the critical current by driving the octupole with 1000 A, setting the external solenoid to 4.2 T, and slowly ramping the mirror current. The octupole quenched repeatedly at approximately the same mirror currents; no obvious training was observed. Using the values of the currents through the respective magnets at the quenches, we calculate that the maximum B_{norm} in the octupole was 4.68 T. This value is plotted in Fig. 2 and fits well with the extrapolation of the short sample data. Thus, we conclude that the short sample current can be attained in the ALPHA octupole.

As mentioned in Section 2.1.4, we do not yet know whether plasmas can be injected while the octupole is on. Moreover, we might wish to detect trapped antihydrogen by quickly turning off the octupole field. Thus, it is essential that the octupole field can be ramped relatively quickly. With no background field, the prototype octupole can be ramped to 1000 A with a ramping speed of $4500\,\mathrm{A s^{-1}}$. Using the same ramp rate the octupole quenches at 930 and 750–830 A for 2 and 4 T background fields, respectively.

If a superconducting magnet and its ancillary protection circuitry are not designed properly, the wire continuity can be destroyed in a quench. A typical quench starts when a small section of the superconducting wire goes normal. Joule heating quickly heats this section, further increasing its resistance and increasing the local power dissipation. Unless there is a lot of copper to bypass the current around the quench, this cycle is unstable and the quench is unstoppable. If the temperature of the resultant hot spot exceeds about 1000 K, the wire can be damaged or destroyed. Temperatures above 500 K will leave the superconducting material intact, but the insulation can be damaged either due to mechanical motion or by the temperature itself.

If the octupole's current drops sufficiently quickly, the energy deposited into the hot spot will be limited, the temperatures will stay below 500 K, and the wire will not be damaged. Both the octupole's stored inductive energy and the octupole's power supply strive to keep the current constant. But both will be unable to do so as the resistance of the magnet rises: the inductive current will decay, and the power supply will voltage limit. A resistance of several tens of milliohms will quickly damp the current. The resistance of the original hot spot itself is not very large, but as the heat from the hot spot spreads, the normal region will grow. The faster the hot spot grows, the higher the octupole's resistance, and the lower the ultimate hot spot temperature. The propagation speed of the normal region boundary is called the quench velocity. The closer the wire is to its critical current, the lower the critical temperature, and the faster the quench will spread. Paradoxically, due to the slower quench velocity, the wire is less likely to be damaged near its critical current than at about half the critical current.

Fig. 8 shows a typical quench velocity measurement. We initiate the quench by powering a spot heater for about 50 ms. Since we can measure the current and the voltage drop across the hot spot, we know its resistivity. At high temperatures (>100 K) the temperature dependence of the resistivity of copper is well specified. Using measurements at 77 K and the superconducting/normal transition, we can calibrate the low-temperature resistivity. Consequently, we can determine the hot spot temperature as a function of the resistivity. Using additional nearby voltage taps, we can also measure the quench propagation velocity.

On the prototype system, we measured quench velocities in the range of $20\text{–}80\,\mathrm{m s^{-1}}$ depending on the octupole current, the external fields, if any, and the location of the quench. The hot spot temperatures ranged up to about 215 K.

5. Quench protection

We detected quenches by monitoring the magnet's resistance; only during quenches will the resistance be non-zero. We determined the resistance by measuring the voltage drop across the inner and outer magnet layers. Scaling and differencing these two measurements nulls the reactive component of the drop, leaving only the resistive component. When we detect a quench, we use an external SCR crowbar to shunt the power supply current. We also command the power supply to turn-off; however, the power supply responds to this command with a delay on the order of 100 ms. As the prototype hotspot temperatures never exceeded 215 K, no external energy extraction was necessary. Fig. 9 shows the time history of a typical, spot-heater initiated, quench. The magnet current before the quench was 923 A. The quench resistance curve, found by dividing the resistive voltage drop across the prototype by

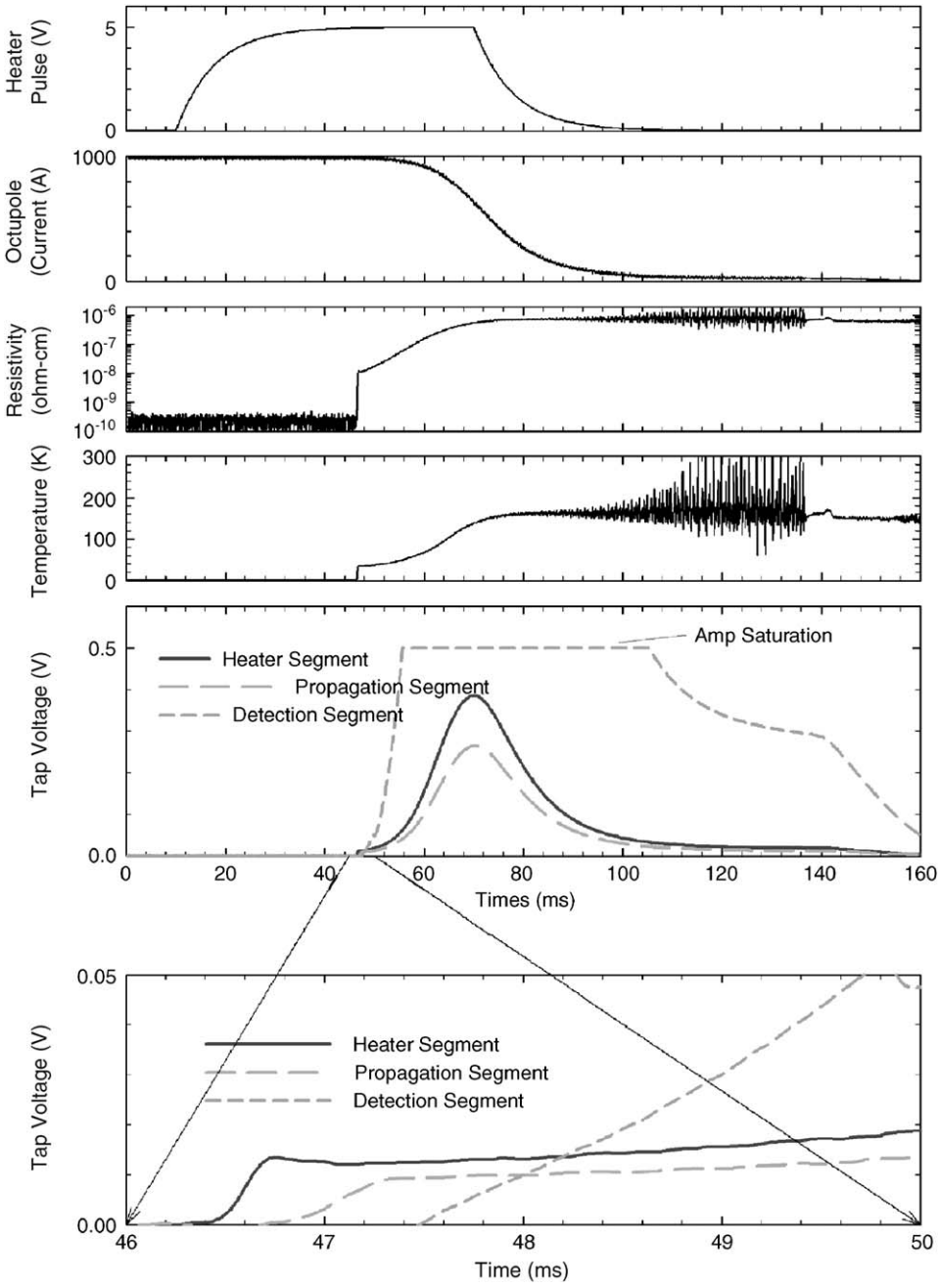

Fig. 8. Typical quench in the octupole prototype. The top graph shows the current in the heater that induces the quench. The next graph shows the decay of the octupole current after the quench, and the third graph shows the growth of the resistivity of the "propagation" segment. The fourth graph displays the temperature of this segment, calculated from the resistivity. The bottom two graphs show the voltages on taps near the quench heater; the quench velocity can be calculated from the difference in onset times between these taps.

the current through the prototype, shows that the resistance increases as the quench spreads. As can be predicted by analytic modeling [37], the resistance initially grows as t^3. Only after the current decays and the heat of the quench begins to diffuse away does the resistance depart from this scaling. During the quench shown in Fig. 3, we delayed firing the SCR and turning off the power supply until 50 ms after the quench. By this time, the KIITS have nearly reached their asymptotic value of 20 kA^2 s. The KIITS are the time-integrated current squared after the quench. In an adiabatic model [38], the dependence of the hot spot temperature on the KIITS becomes exponential at high temperatures (hundreds of Kelvin). At lower temperatures, the dependence follows no simple scaling, but can be fit to a monotonic, third order polynomial. The fit constants depend on the cable, but, for a given cable, can be empirically determined by correlating KIITS measurements with hot spot temperatures. Once these constants are determined, measured or predicted values of the KIITS can be used to infer the hot spot temperature in new operating

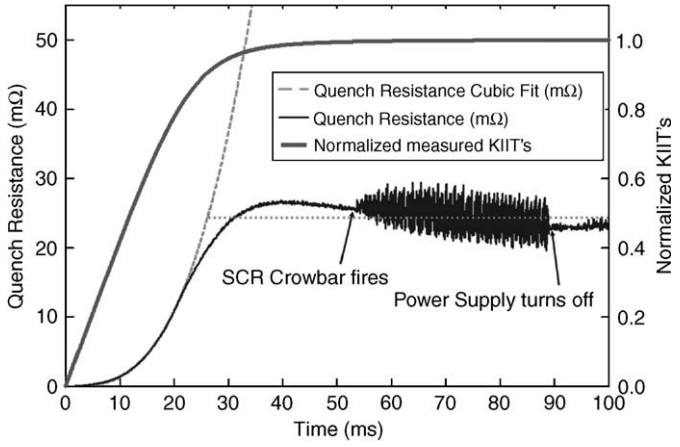

Fig. 9. Induced quench in the prototype at 923 A ($t = 0$ is the quench time). Initially, the quench resistance (the thin solid blue line) increases cubically with time as the dashed line. The saturated value of the resistance used in the Micro-cap simulations is shown by the dashed red horizontal line. The instantaneous measured KIITS (see text), normalized to one, are indicated by the thick solid green line. In this specific run the quench protection was purposefully delayed by 50 ms. We can determine when the SCR fires and when the power supply turns off from the noise on the resistance curve, and these points are indicated on the diagram.

regimes. The KIITS in the prototype were always less than 25 $kA^2 s$ with hot spot temperatures at most around 215 K, not yet in the purely exponential regime. Therefore, extrapolation to higher KIITS and much higher temperatures is approximate. In order to estimate the KIITS, and hence the hotspot temperature, for the final magnet design, we simulated the system with the electrical circuit simulation program Micro-cap [39]. We calibrated the model by fitting it to the prototype measurements. We found that we best matched the measured KIITS when we saturated the resistance at the point where the simulation KIITS in the non-saturated case reached 95% of their asymptotic value. Thus, the simulations had two steps for each parameter set: first, with a non-saturated resistance to determine the saturated resistance; and second, with no more than the saturated resistance to determine the final predicted KIITS.

Measurements described in Section 4 show that, in the prototype, our wire is intrinsically protected in a quench, and does not require any external protection. However, the inductance of the eight layer ALPHA octupole (4 mH) is more than 10 times greater than the inductance of the two layer prototype (0.3 mH), and it will run at 10% more current. Consequently, there will be about 12 times more energy stored in the ALPHA octupole than in the prototype. This could lead to dangerous hot spot temperatures.

To estimate the ALPHA hot spot temperature, we ran our Micro-Cap simulation with the ALPHA octupole parameters. The increased current is expected to increase the quench propagation velocity, and this effect will help ameliorate the effect of the greater stored energy. To model the resistance time dependence, we use Eq. (9.54) of [37], which, with some further manipulations, gives the following scaling for the quench resistance as a function of time,

$$R(t) \propto N I_0^4 v t^3 \tag{3}$$

where N is the number of layers, I_0 is the initial current in the magnet and v is the quench propagation velocity. By extrapolating the measured prototype quench propagation velocities to the higher currents used in the ALPHA octupole, we estimate that the propagation velocity will be at least 25% higher in ALPHA. The quench velocity may be even higher because B_{norm} will be higher in the ALPHA octupole than in the prototype. To cover all possibilities, we modeled the ALPHA octupole assuming increases of 0%, 25% and 50% in the velocity.

The Micro-Cap simulation gave a KIITS of 32.4 $kA^2 s$ for the original quench propagation velocity, 30.7 $kA^2 s$ for a 25% increase in the velocity and 29.3 $kA^2 s$ for the 50% increase. Extrapolating the prototype KIITS/hot spot measurements, as shown in Fig. 10, yields hot spot temperatures from around 400 K for the 50% case to around 600 K for the 0% case. As these temperatures are close to the conservative safety limit of 500 K, we will use active quench protection with external energy extraction on the ALPHA octupole.

The four superconducting coils in the ALPHA cryostat will be protected by a quench protection system featuring fast energy extraction enabled by an IGBT (insulated gate bipolar transistor) switch [40]. Quenches will be detected by a field-programmable gate array based magnet control system, which monitors voltage drops in the coils, across the superconducting bus bars and in the vapor cooled leads which feed the coils. When a quench is detected, the power supply will be crow-barred using an SCR switch, and the IGBT will divert the magnet current to a dump resistor. The time scale for the current decay in the octupole circuit

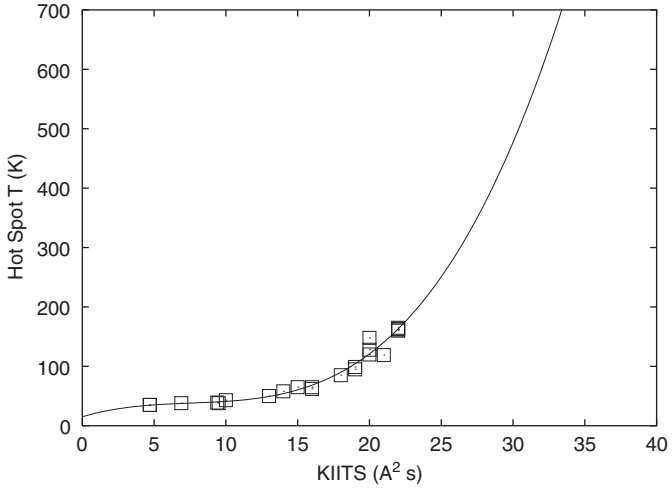

Fig. 10. Dependence of the hot spot temperature on the KIITS. The prototype data are marked by squares, up to 23 KIITS and 215 K. A polynomial fit (third order) is plotted (solid line) and extrapolated up to 32.5 KIITS. Due to the predicted exponential growth at high temperatures the extrapolation is only approximate.

will be about 10 ms. It is anticipated that the same circuit can be used for controlled, fast turn-off of the magnetic trap without quenching, but tests on this have not yet been conducted. Provisions for active quench protection using pulsed heaters to distribute the quench are also built into the coils.

6. Conclusions

We have given a comprehensive description of a magnetic trap for antihydrogen confinement comprising an octupole and mirror coil arrangement, together with a solenoid to facilitate initial antiproton capture. The detailed design criteria and issues which have informed our choice of this system have been elucidated. The novel wire and winding arrangements used to produce the trap, which is 1.16 T deep, have been described.

Quench tests on a prototype octupole coil have been used to extrapolate the performance to the final coil system. This has dictated the use of external quench protection for the system as deployed in the ALPHA antihydrogen apparatus.

Acknowledgments

This work was supported by the NSF and by the EPSRC, UK(EP/D038707/1). We thank J. Muratore for discussions of quench threshold modeling, A. Marone and M. Anerella for mechanical and coil production design considerations and G. Ganetis for discussions relating to quench protection. We are also grateful to A. Lietzke, A. McInturff, the LBNL Superconducting Magnet Group and the LBNL Building 58 Staff. Furthermore we would like to thank F. Fowler and S. Russenschuck.

References

[1] G. Luders, Ann. Phys. 2 (1957) 1.
[2] R. Bluhm, A. Kostelecký, N. Russell, Phys. Rev. Lett. 82 (1999) 2254.
[3] M. Charlton, J. Eades, D. Horvath, R.J. Hughes, C. Zimmermann, Phys. Rep. 241 (1994) 65.
[4] G.M. Shore, Nucl. Phys. B 717 (2005) 86.
[5] M. Amoretti, et al., Nature 419 (2002) 456.
[6] M. Amoretti, et al., Phys. Lett. B 578 (2004) 23.
[7] G. Gabrielse, et al., Phys. Rev. Lett. 89 (2002) 213401.
[8] N. Madsen, et al., Phys. Rev. Lett. 94 (2005) 033403.
[9] G. Gabrielse, et al., Phys. Rev. Lett. 93 (2004) 073401.
[10] F. Robicheaux, Phys. Rev. A 70 (2004) 022510.
[11] C.H. Storry, et al., Phys. Rev. Lett. 93 (2004) 263401.
[12] ⟨http://doc.cern.ch//archive/electronic/cern/preprints/spsc/public/spsc-2005-006.pdf⟩.
[13] B.I. Deutch, et al., Phys. Scr. T22 (1988) 248.
[14] G. Gabrielse, et al., Phys. Lett. A 129 (1988) 38.
[15] D.H.E. Dubin, Phys. Plasmas 8 (2001) 4331.
[16] C.A. Ordonez, D.D. Dolliver, Y. Chang, J.R. Correa, Phys. Plasmas 9 (2002) 3289.
[17] J. Fajans, A. Schmidt, Nucl. Instr. and Meth. A 521 (2004) 318.
[18] F. Robicheaux, Phys. Rev. A 73 (2006) 033401.
[19] M. Amoretti, et al., Nucl. Instr. and Meth. A 518 (2004) 679.
[20] C.L. Taylor, J. Zhang, F. Robicheaux, Cooling of Rydberg antihydrogen during radiative cascade, Phys. Rev. A (2006), submitted for publication.
[21] T.E. Bergeman, G. Erez, H.J. Metcalf, Phys. Rev. A 35 (1987) 1535.
[22] D.E. Pritchard, Phys. Rev. Lett. 51 (1983) 1336.
[23] T.M. O'Neil, Phys. Fluids 23 (1980) 2216.
[24] E.P. Gilson, J. Fajans, in: J. Bollinger, R. Spencer, R. Davidson (Eds.), Non-neutral Plasma Physics III, vol. 498, American Institute of Physics, New York, 1999, p. 250.
[25] E.P. Gilson, J. Fajans, Phys. Rev. Lett. 90 (2003) 015001.
[26] M. Holzscheiter, M. Charlton, M.M. Nieto, Phys. Rep. 402 (2004) 1.
[27] T.M. Squires, P. Yesley, G. Gabrielse, Phys. Rev. Lett. 86 (2001) 5266.
[28] G. Gabrielse, Adv. At. Mol. Opt. Phys. 50 (2005) 155.
[29] J. Fajans, W. Bertsche, K. Burke, S.F. Chapman, D.P. van der Werf, Phys. Rev. Lett. 95 (2005) 155001.
[30] M.C. Fujiwara, AIP Proc. 793 (2005) 111.
[31] SUPERCON, Inc., 830 Boston Turnpike, Shrewsbury, MA 01545.
[32] K. Gomberoff, The ALPHA Collaboration, 2006, to be published.
[33] A.V. Dudarev, V.E. Keilin, N.Ph. Kopeikin, I.O. Shugaev, A.V. Stepanenko, V.V. Stepanov, J. Fajans, D. Durkin, Superconducting Magnet for Non-Neutral Plasma Research, MT-15, 1997.
[34] ⟨http://www.bnl.gov/magnets/BEPCII/BEPCII.asp⟩.
[35] C.F. Driscoll, K.S. Fine, J.H. Malmberg, Phys. Fluids 29 (1986) 2015.
[36] Commercial Product from Vector Fields: ⟨http://www.vectorfields.com/⟩.
[37] M.N. Wilson, Superconducting Magnets, Oxford University Press, Oxford, 1983 (Chapter 9.4).
[38] B.J. Maddock, G.B. James, Proc. Inst. Elect. Eng. 115 (1968) 543.
[39] Micro-Cap 8.0.9.0 Evaluation Version, Copyright (c) 1982–2004 Spectrum Software, ⟨http://www.spectrum-soft.com/index.shtm⟩.
[40] Private communication with G. Ganetis from BNL.